Electronic Structure of Sodium Superoxide Bulk, (100) Surface, and Clusters using Hybrid Density Functional: Relevance for Na–O2 Batteries

ARTICLE *in* JOURNAL OF PHYSICAL CHEMISTRY LETTERS · MAY 2015

Impact Factor: 7.46 · DOI: 10.1021/acs.jpclett.5b00814

4 AUTHORS:

Oier Arcelus
CIC Energigune
1 PUBLICATION **3** CITATIONS
SEE PROFILE

Chunmei Li
CIC Energigune
5 PUBLICATIONS **55** CITATIONS
SEE PROFILE

Teofilo Rojo
Universidad del País Vasco / Euskal Herriko …
554 PUBLICATIONS **9,310** CITATIONS
SEE PROFILE

Javier Carrasco
Spanish National Research Council
50 PUBLICATIONS **1,599** CITATIONS
SEE PROFILE

THE JOURNAL OF PHYSICAL CHEMISTRY Letters

Letter

pubs.acs.org/JPCL

Electronic Structure of Sodium Superoxide Bulk, (100) Surface, and Clusters using Hybrid Density Functional: Relevance for Na−O_2 Batteries

Oier Arcelus,[†] Chunmei Li,[†] Teófilo Rojo,[†,‡] and Javier Carrasco*[,†]

[†]CIC Energigune, Albert Einstein 48, 01510 Miñano, Álava, Spain

[‡]Departamento de Química Inorgánica, Facultad de Ciencia y Tecnología, Universidad del País Vasco UPV/EHU, 48080 Bilbao, Spain

Supporting Information

ABSTRACT: Clarifying the electronic structure of sodium superoxide (NaO_2) is a key step in understanding the electrochemical behavior of Na−O_2 batteries. Here we report a density functional theory study to explore the effect of atomic structure and morphology on the electronic properties of different model systems: NaO_2 bulk, (100) surface, and small $(NaO_2)_n$ clusters (n = 3−8). We found that a correct description of the open-shell 2p electrons of O_2^- requires the use of a hybrid functional, which reveals a clear insulating nature of all of the investigated systems. This sheds light onto the capacity limitations of pure NaO_2 as a discharge product and highlights the need for developing new strategies to enhance its electron transport in the optimization of Na−O_2 cells.

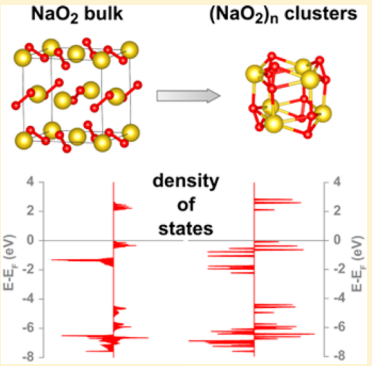

Metal-air batteries are attractive energy storage devices for electrifying transportation because they can theoretically store far more energy than most competing technologies. The high energy density of metal-air batteries is achieved by reducing the oxygen in the air rather than storing it through intercalation mechanisms, as occurs in conventional energy storage technologies.[1] A prominent example of metal-air batteries is the Li−O_2 cell,[2−4] with a theoretical energy density of 3.5 kWh/kg; this is 5 to 10 times higher than that of present Li-ion cells and almost comparable to that of petrol;[5] however, one of the problems preventing its widespread commercialization is the large polarization on discharge and charge.[6] Substituting lithium by other alkali metals (Na and K) has recently emerged as a feasible approach to overcome this shortcoming;[7−10] however, there remains much to be understood in terms of unveiling the molecular-level mechanisms of discharge products formation during the oxygen reduction reaction (ORR)[11,12] and in using this fundamental insight into improving alkali metal-air battery technologies.

For the Na−O_2 system, Hartmann et al.[7,11] have recently demonstrated the formation of a stable sodium superoxide at the end of discharge, with particles size of 1−50 μm; however, these laboratory-scale experiments show strong capacity fading. Capacity loss is strongly related to the underlying crystal growth mechanisms of the discharge product. Hence it would be particularly relevant to clarify whether O_2 is reduced on the cathode support (typically carbon) or directly on NaO_2 surface sites during the ORR. Considering the large size of the formed particles, in the former mechanism the generated O_2^- species would have to dissolve in the electrolyte and diffuse to the growing NaO_2 crystal in the solution, whereas the latter mechanism would require sufficient electrical conductivity of NaO_2.[13] Shedding light into this issue can ultimately help to advance the fundamental understanding of Na−O_2 batteries and their future development. It is therefore interesting and timely to investigate the electronic structure of NaO_2. We have explored the electronic structure of different NaO_2 materials models: bulk, extended surface, and small clusters using density functional theory (DFT). The aim of considering this range of NaO_2 systems is two-fold: (i) to investigate how different morphologies alter the electronic structure of the material and (ii) to obtain a better understanding of particle size effects when going from small clusters (early stages of NaO_2 formation) to extended surfaces (advanced stages of NaO_2 growth).

We performed spin-polarized DFT calculations using the Perdew−Burke−Ernzerhof (PBE) gradient-corrected functional[14] and the Heyd−Scuseria−Ernzerhof (HSE06) hybrid density functional with 25% exact Hartree−Fock exchange.[15] Calculations were carried out using the Vienna ab initio simulation package (VASP) 5.3 code.[16−18] In all cases we replaced the core electrons by PBE-based projector-augmented wave (PAW) potentials,[19] whereas we treated explicitly the Na ($2p^6$ $3s^1$) and O ($2s^2$ $2p^4$) electrons as valence electrons, and

Received: April 20, 2015
Accepted: May 11, 2015

DOI: 10.1021/acs.jpclett.5b00814
J. Phys. Chem. Lett. 2015, 6, 2027−2031

their wave functions were expanded in plane-waves with a cutoff energy of 500 eV. All of the geometries were optimized with a residual forces threshold of 0.02 eV/Å. Further computational details are provided in the Supporting Information (SI).

Bulk NaO_2. Between 196 and 223 K, NaO_2 crystallizes in the cubic $Pa\bar{3}$ space group (pyrite phase), with O_2^- molecular bond axes parallel to the ⟨111⟩ directions (Figure 1a).[20] Upon heating above 223 K, O_2^- species freely rotate to have a $Fm\bar{3}m$ structure.[20] Such O_2^- orientation disorder of NaO_2 is therefore expected to occur in Na−O_2 cells under working conditions. Nevertheless, in this study we approximated the NaO_2 structure to that of the ordered pyrite phase. First, we optimized the equilibrium lattice parameters of bulk NaO_2, allowing the atomic positions, lattice constants, and cell shape to relax. Both PBE and HSE06 yield lattice parameters (a_{PBE} = 5.509 Å and a_{HSE06} = 5.487 Å) close to the experiment (5.460 Å).[20] The O_2 bond lengths are also very similar between the two functionals: 1.354 (PBE) and 1.326 Å (HSE06); however, the electronic structure predicted by PBE and HSE06 differs significantly. Figure 2a shows the partial density of states (PDOS) projected onto the p orbitals of oxygen atoms using PBE. If one considers the molecular orbital (MO) diagram of the O_2^- molecule, the low-energy states that appear around 4.5 to 6 and 6 to 7 eV below the Fermi level (E_F) correspond to σ_g- and π_u-like bonding MOs, respectively. The empty states above 4.2 eV are σ_u*-like antibonding MOs, whereas the π_g*-like antibonding MOs appears around E_F. A key observation is that NaO_2 is insulating in the spin-up channel, but spin-down π_g* states form a narrow, half-filled band, which would make NaO_2 a half-metallic material. Solovyev et al. recently reported a similar electronic structure using the local density approximation;[21] however, switching to HSE06 (Figure 2b) splits the degeneracy of π_g* states, with the formation of one fully occupied state immediately below E_F and one empty state around 2.0 to 2.5 eV above it. This is in good qualitative agreement with the HSE06 calculations reported by Lee and coworkers.[22] Overall, the HSE06 functional predicts an insulating character for NaO_2 in contrast with PBE.

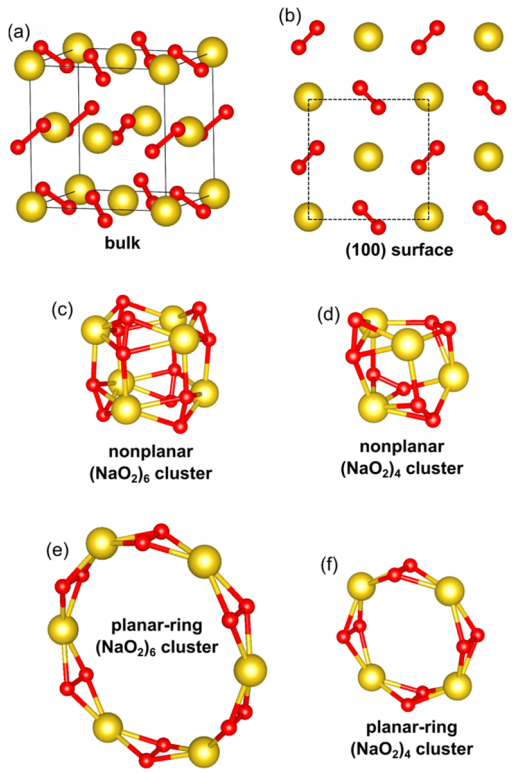

Figure 1. Optimized structures of (a) $Pa\bar{3}$ NaO_2 bulk, (b) NaO_2(100) surface (top view), (c,d) nonplanar $(NaO_2)_6$ and $(NaO_2)_4$ clusters, and (e,f) planar-ring $(NaO_2)_6$ and $(NaO_2)_4$ clusters. Yellow and red spheres are Na and O atoms, respectively.

We also included the on-site Coulomb interaction between O 2p electrons using Hubbard U corrections (PBE+U), which is computationally much less demanding than the HSE06 approach. Increasing the U term results in a larger splitting of π_g* states between spin up and spin down (Figure S1 in the SI); however, the spin-down states are still degenerated and the system remains half-metallic. Kim et al.[23] reported a similar failure of PBE+U to satisfactorily reproduce the insulating character of body-centered tetragonal KO_2, which is a more symmetric structure than the pyrite phase, with all O_2^- molecular bond axes parallel to the ⟨001⟩ directions. Interestingly, PBE+U opens the band gap in KO_2 when lowering the symmetry of the crystal by the tilting of O_2^- species.[23] This is in contrast with the case of NaO_2, where we observed that the combined effect of the Coulomb U term and the crystal field from Na^+ ions is unable to split the π_g* states. Therefore, for the correct description of the insulating electronic structure of pyrite NaO_2, the use of a hybrid functional such as HSE06 is necessary, whereas PBE or PBE+U yield metallic behavior.

NaO_2(100) Surface. Our HSE06 results show that NaO_2 is a bulk insulator, but surface states might affect the electronic conductivity. Conductive surface pathways have actually been proposed for stable surfaces of discharge products in Li−O_2 batteries. In particular, Radin et al.[24,25] have identified magnetic surface oxygen atoms for the Li_2O_2 (0001) surface despite the insulating character of bulk Li_2O_2. Therefore, it is interesting to explore the possible existence of similar conducting channels for NaO_2. According to scanning electron microscopy (SEM) images from Hartmann et al.,[11] the NaO_2 discharge product mainly consists of well-defined cubic shape particles, most probably composed of stoichiometric {100} facets. Lee et al.[22] and Kang et al.[26] have showed that the (100) orientation is indeed the most stable low-index surface of pyrite NaO_2, with the specific stoichiometric termination shown in Figure 1b. The calculated layer-projected PDOS of this surface using PBE is shown in Figure 2c. Similar to bulk NaO_2, the spin-up states are insulating, while the spin-down states show a half-metallic character. Furthermore, the system shows ferromagnetic behavior, which, as in the bulk, arises from an unpaired π_g* electron on each superoxide ion. Again, HSE06 recovers the insulating nature of the system (Figure 2d). We found that the HSE06 band gap for the three topmost layers of the NaO_2(100) surface (1.9 eV) is very similar to that of the bulk phase (2.1 eV). This result points out that the electronic conductivity of the clean (100) surface and bulk should not differ significantly. Interestingly, the O 2p states of the first surface layer (red solid line in Figure 2d) appear as a sharp peak at 2.7 eV above E_F, which indicates that this first layer actually contributes to electrically passivate the surface. Overall, our analysis suggests that particle morphologies exhibiting extended (100) surfaces or grain boundaries are not expected to be beneficial to improve the conducting properties of NaO_2.

DOI: 10.1021/acs.jpclett.5b00814
J. Phys. Chem. Lett. 2015, 6, 2027−2031

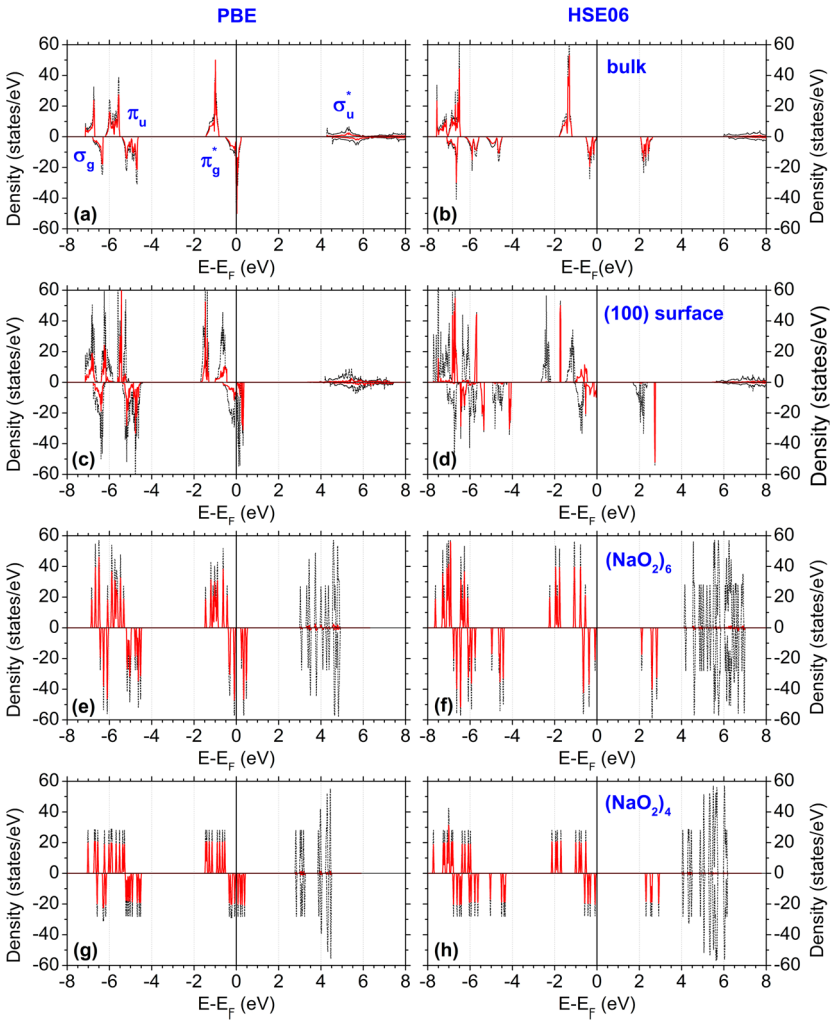

Figure 2. Density of states for (a,b) bulk NaO_2, (c,d) NaO_2(100) surface, (e,f) nonplanar $(NaO_2)_6$ cluster, and (g,h) nonplanar $(NaO_2)_4$ cluster. The black dashed (red solid) lines are the total DOS (PDOS projected onto the p orbitals of oxygen atoms). In the case of the NaO_2(100) surface, the PDOS is projected onto the oxygen atoms of the topmost surface layer (red solid line), whereas the black dashed line accounts for the PDOS projected onto the three topmost surface layers. Positive (negative) values correspond to spin up (down) states. Two different functionals are considered: PBE (left) and HSE06 (right). The energy zero is E_F.

NaO_2 Small Clusters. Particle size and shape also significantly impact the electrochemical performance of electroactive materials.[27] For example, nanosized crystals often help to reduce transport path lengths or enhance electric field distributions. (See ref 28 for a recent review.) Thus, it is of interest to investigate the electronic structure of small NaO_2 clusters as they may participate in the early stages of nucleation and growth of discharge products. Das et al.[29] have investigated the structure and stability of gas-phase $(LiO_2)_n$ clusters (n = 1−12, 16, 18) akin to $(NaO_2)_n$. Lithium superoxide clusters prefer to form planar-ring structures up to n = 12. Three-dimensional, nonplanar geometries are always less stable than planar rings, but energy differences between them gradually decay with cluster size and nonplanar isomers become energetically favorable after n = 12. For sodium superoxide clusters, we found that the onset of preference for nonplanar geometries happens before: nonplanar $(NaO_2)_n$ isomers (Figure 1c,d) already start to be preferred over planar-ring structures (Figure 1e,f) around n = 4−6. Table 1 gives the computed formation energies of $(NaO_2)_3$, $(NaO_2)_4$, $(NaO_2)_6$, and $(NaO_2)_8$. Essentially, PBE and HSE06 yield almost identical formation energies (the inclusion of zero-point energy in the calculations has a minor effect, reducing the formation energy by 20−30 meV) and interatomic distances, with differences <0.037 Å (Table S1 in the SI). Both functionals predict nearly degenerated stabilities of planar-ring and nonplanar isomers for $(NaO_2)_4$, $(NaO_2)_6$, and $(NaO_2)_8$ clusters; formation energy differences range between 10 and 80 meV.

Table 1. Calculated Formation Energies (in eV per NaO_2 Unit) of $(NaO_2)_3$, $(NaO_2)_4$, $(NaO_2)_6$, and $(NaO_2)_8$ Clusters Using PBE and HSE06[a]

	geometry	PBE	HSE06
$(NaO_2)_3$	planar-ring	−1.20 (−1.18)	−1.23 (−1.21)
$(NaO_2)_4$	planar-ring	−1.32 (−1.29)	−1.35 (−1.33)
	nonplanar	−1.27 (−1.25)	−1.27 (−1.25)
$(NaO_2)_6$	planar-ring	−1.39 (−1.37)	−1.43 (−1.41)
	nonplanar	−1.43 (−1.41)	−1.42 (−1.40)
$(NaO_2)_8$	planar-ring	−1.42	−1.46
	nonplanar	−1.48	−1.50

[a]Values in parentheses are zero-point-corrected energies.

We now consider the $(NaO_2)_4$ and $(NaO_2)_6$ clusters to explore their electronic structure and compare them with those

DOI: 10.1021/acs.jpclett.5b00814
J. Phys. Chem. Lett. 2015, 6, 2027−2031

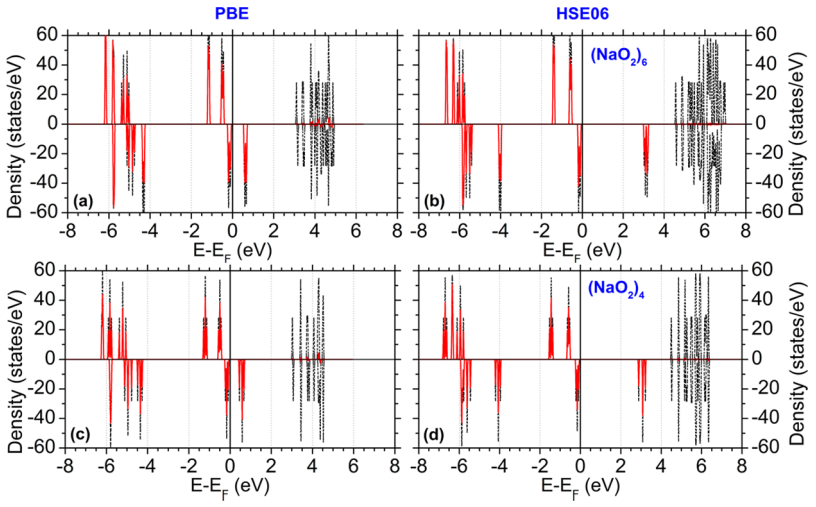

Figure 3. Density of states for (a,b) planar-ring $(NaO_2)_6$ cluster and (c,d) planar-ring $(NaO_2)_4$ cluster. The black dashed (red solid) lines are the total DOS (PDOS projected onto the p orbitals of oxygen atoms). Positive (negative) values correspond to spin up (down) states. Two different functionals are considered: PBE (left) and HSE06 (right). The energy zero is E_F.

of extended systems. First we focus on nonplanar isomers because they present a more bulk-like structure than planar rings. Figure 2e–h shows the corresponding PDOS computed with PBE and HSE06. The discretization of bands, which occurs when moving from NaO_2 bulk and (100) surface to small clusters, indeed has a minor impact on the relative position of the peaks and general band structure below E_F; however, the PBE (HSE06) onset of empty σ_u*-like states at 4.2 (6.0) eV above E_F in NaO_2 bulk (Figure 2a,b) is shifted to lower energies by ca. 1.2 (1.9) eV for both $(NaO_2)_6$ and $(NaO_2)_4$ clusters. Again, PBE places the empty spin-down π_g* states near E_F, but HSE06 opens the gap and the first $(NaO_2)_6$ and $(NaO_2)_4$ unoccupied state appears at 2.0 and 2.3 eV above E_F, respectively. Similarly to the bulk and (100) surface previously discussed, these results indicate that nonplanar clusters are expected to behave as insulator materials, too.

Planar-ring clusters exhibit less-coordinated O_2^- species to Na atoms than nonplanar clusters. That impacts their electronic structure, resulting in significant differences between the two geometries. Interestingly, PBE splits the occupied and unoccupied π_g* states for both $(NaO_2)_6$ and $(NaO_2)_4$ clusters (Figure 3a,c), opening a gap of ∼0.5 eV and therefore resulting in a well-defined insulating system. This is in contrast with nonplanar clusters, where PBE places the unoccupied π_g* states much closer to E_F, especially in the case of $(NaO_2)_4$ (Figure 2g). The HSE06 energy gap between the highest occupied and lowest unoccupied π_g* states for both $(NaO_2)_6$ and $(NaO_2)_4$ is actually enlarged even further, up to almost 3 eV (Figure 3b,d). In addition, the HSE06 energy gap is ∼1 eV larger than the gap computed for nonplanar clusters (Figure 2f,h). These results indicate that planar-ring clusters are indeed more insulating than nonplanar clusters, the bulk, and the (100) surface.

In conclusion, we have reported a DFT study of the electronic structure of NaO_2 using several materials models ranging from bulk, extended (100) surface and different $(NaO_2)_n$ clusters (n = 4,6). Our results show the formation of fully occupied spin-up and half-filled spin-down antibonding states in the valence band of all these systems. These states are associated with the O_2^- species. The conventional PBE functional and PBE+U approach essentially predict a half-metallic character for the bulk, (100) surface and clusters with highly coordinated O_2^- species; however, we found that for a suitable description of the partially occupied O 2p states the hybrid HSE06 functional is required. This result highlights the failure of conventional generalized gradient approximations to qualitatively describe open-shell 2p electrons in the investigated superoxide systems. By using HSE06 we find that the empty O 2p states indeed appear well above the Fermi level, with band gaps larger than ∼2 eV. Therefore, all investigated systems are expected to exhibit insulating character. This result provides valuable insight into the fundamental understanding of the electrocrystallization of NaO_2 in Na-air batteries. The absence of effective electron conductive pathways along the most stable (100) surface and small clusters indicates that O_2 reduction should occur at the interface between the electrolyte and the conducting cathode support instead of directly on growing NaO_2 particles. In a broader context this study raises the possibility of interesting follow-on studies to enhance charge transport trough doping or the engineering of the NaO_2–carbon interface to achieve high-specific-energy Na-air batteries. For example, recent systematic studies using commercial carbon material showed that the morphology of the discharge product is strongly affected by the surface topology and pore size of the carbon substrate.[30] This indicates that surface defects and structure can play an important role in the functioning of Na-air batteries. In general, comparison of first-principle methods on these and other materials models along with accurate electrochemical measurements on the crystalline growth of NaO_2 remains highly desirable.

■ ASSOCIATED CONTENT

Supporting Information

Detailed results (computational details, density of states using PBE+U, interatomic distances, and optimized coordinates of atomic structures). The Supporting Information is available free of charge on the ACS Publications website at DOI: 10.1021/acs.jpclett.5b00814.

■ AUTHOR INFORMATION

Corresponding Author

*E-mail: jcarrasco@cicenergigune.com. Tel: +34 94 529-7108.

DOI: 10.1021/acs.jpclett.5b00814
J. Phys. Chem. Lett. 2015, 6, 2027–2031

Notes

The authors declare no competing financial interest.

■ ACKNOWLEDGMENTS

Computer time provided by the Barcelona Supercomputer Center (BSC), i2BASQUE, and the Supercomputing Center of Galicia (CESGA) is acknowledged. J.C. is supported by the MINECO through a Ramón y Cajal Fellowship and acknowledges support by the Marie Curie Career Integration Grant FP7-PEOPLE-2011-CIG: Project NanoWGS and The Royal Society through the Newton Alumnus scheme.

■ REFERENCES

(1) Whittingham, M. S. Lithium Batteries and Cathode Materials. *Chem. Rev.* **2004**, *104*, 4271−4301.
(2) Abraham, K. M.; Jiang, Z. A. Polymer Electrolyte-Based Rechargable Lithium/Oxygen Battery. *J. Electrochem. Soc.* **1996**, *143*, 1−5.
(3) Girishkumar, G.; McCloskey, B.; Luntz, A. C.; Swanson, S.; Wilcke, W. Lithium-Air Battery: Promise and Challenges. *J. Phys. Chem. Lett.* **2010**, *1*, 2193−2203.
(4) Bruce, P. G.; Freunberger, S. A.; Hardwick, L. J.; Tarascon, J. M. Li−O_2 and Li−S Batteries with High Energy Storage. *Nat. Mater.* **2012**, *11*, 19−29.
(5) Zhang, T.; Zhou, H. From Li−O_2 to Li−Air Batteries: Carbon Nanotubes/Ionic Liquid Gels with a Tricontinuous Passage of Electrons, Ions, and Oxygen. *Angew. Chem., Int. Ed.* **2012**, *51*, 11062−11067.
(6) Peng, Z. Q.; Freunberger, S. A.; Chen, Y.; Bruce, P. G. A Reversible and Higher-Rate Li-O_2 Battery. *Science* **2012**, *337*, 563−566.
(7) Peled, E.; Golodnitsky, D.; Mazor, H.; Goor, M.; Avshalomov, S. Parameter Analysis of a Practical Lithium- and Sodium-Air Electric Vehicle Battery. *J. Power Sources* **2011**, *196*, 6835−6840.
(8) Hartmann, P.; Bender, C. L.; Vracar, M.; Durr, A. K.; Garsuch, A.; Janek, J.; Adelhelm, P. A Rechargeable Room-Temperature Sodium Superoxide (NaO_2) Battery. *Nat. Mater.* **2013**, *12*, 228−232.
(9) Ren, X.; Wu, Y. A Low-Overpotential Potassium−Oxygen Battery Based on Potassium Superoxide. *J. Am. Chem. Soc.* **2013**, *135*, 2923−2926.
(10) McCloskey, B. D.; Garcia, J. M.; Luntz, A. C. Chemical and Electrochemical Differences in Non-aqueous Li-O_2 and Na-O_2 Batteries. *J. Phys. Chem. Lett.* **2014**, *5*, 1230−1235.
(11) Hartmann, P.; Bender, C. L.; Sann, J.; Durr, A. K.; Jansen, M.; Janek, J.; Adelhelm, P. A. Comprehensive Study on the Cell Chemistry of the Sodium Superoxide (NaO2) Battery. *Phys. Chem. Chem. Phys.* **2013**, *15*, 11661−11672.
(12) Ren, X.; Lau, K. C.; Yu, M.; Bi, X.; Kreidler, E.; Curtiss, L. A.; Wu, Y. Understanding Side Reactions in K-O_2 Batteries for Improved Cycle Life. *ACS Appl. Mater. Interfaces* **2014**, *6*, 19299−19307.
(13) Johnson, L.; Li, C.; Liu, Z.; Chen, Y.; Freunberger, S. A.; Ashok, P. C.; Praveen, B. B.; Dholakia, K.; Tarascon, J.-M.; Bruce, P. G. The Role of LiO_2 Solubility in O_2 Reduction in Aprotic Solvents and its Consequences for Li−O_2 Batteries. *Nat. Chem.* **2014**, *6*, 1091−1099.
(14) Perdew, J.; Burke, K.; Ernzerhof, M. Generalized Gradient Approximation Made Simple. *Phys. Rev. Lett.* **1996**, *77*, 3865−3868.
(15) Krukau, A. V.; Vydrov, O. A.; Izmaylov, A. F.; Scuseria, G. E. Influence of the Exchange Screening Parameter on the Performance of Screened Hybrid Functionals. *J. Chem. Phys.* **2006**, *125*, 224106-1−224106-5.
(16) Kresse, G.; Hafner, J. Ab Initio Molecular-Dynamics for Liquid-Metals. *Phys. Rev. B* **1993**, *47*, 558−561.
(17) Kresse, G.; Furthmüller, J. Efficient Iterative Schemes for Ab Initio Total-Energy Calculations Using a Plane-Wave Basis Set. *Phys. Rev. B* **1996**, *54*, 11169−11186.
(18) Kresse, G.; Furthmüller, J. Efficiency of Ab-Initio Total Energy Calculations for Metals and Semiconductors using a Plane-Wave Basis Set. *Comput. Mater. Sci.* **1996**, *6*, 15−50.
(19) Kresse, G.; Joubert, D. From Ultrasoft Pseudopotentials to the Projector Augmented-Wave Method. *Phys. Rev. B* **1999**, *59*, 1758−1775.
(20) Wriedt, H. A. The Na−O (Sodium-Oxygen) System. *Bull. Alloy Phase Diagrams* **1987**, *8* (3), 234−246.
(21) Solovyev, I. V.; Pchelkina, Z. V.; Mazurenko, V. V. Magnetism of Sodium Superoxide. *CrystEngComm* **2014**, *16*, 522−531.
(22) Lee, B.; Seo, D.-H.; Lim, H.-D.; Park, I.; Park, K. Y.; Kim, J.; Kang, K. First-Principles Study of the Reaction Mechanism in Sodium-Oxygen Batteries. *Chem. Mater.* **2014**, *26*, 1048−1055.
(23) Kim, M.; Kim, B. H.; Choi, H. C.; Min, B. I. Antiferromagnetic and Structural Transitions in the Superoxide KO_2 from First Principles: A 2p-Electron System with Spin-Orbital-Lattice Coupling. *Phys. Rev. B* **2010**, *81*, 100409-1−100409-4.
(24) Radin, M. D.; Rodriguez, J. F.; Tian, F.; Siegel, D. J. Lithium Peroxide Surfaces Are Metallic, While Lithium Oxide Surfaces Are Not. *J. Am. Chem. Soc.* **2012**, *134*, 1093−1103.
(25) Radin, M. D.; Tian, F.; Siegel, D. J. Electronic Structure of Li_2O_2 (0001) Surfaces. *J. Mater. Sci.* **2012**, *47*, 7564−7570.
(26) Kang, S. Y.; Mo, Y.; Ong, S. P.; Ceder, G. Nanoscale Stabilization of Sodium Oxides: Implications for Na-O_2 Batteries. *Nano Lett.* **2014**, *14*, 1016−1020.
(27) Bruce, P. G.; Scrosati, B.; Tarascon, J. M. Nanomaterials for Rechargeable Lithium Batteries. *Angew. Chem., Int. Ed.* **2008**, *47*, 2930−2946.
(28) Islam, M. S.; Fisher, C. A. J. Lithium and Sodium Battery Cathode Materials: Computational Insights into Voltage, Diffusion and Nanostructural Properties. *Chem. Soc. Rev.* **2014**, *43*, 185−204.
(29) Das, U.; Lau, K. C.; Redfern, P. C.; Curtiss, L. A. Structure and Stability of Lithium Superoxide Clusters and Relevance to Li-O_2 Batteries. *J. Phys. Chem. Lett.* **2014**, *5*, 813−819.
(30) Yadegari, H.; Li, Y.; Banis, M. N.; Li, X.; Wang, B.; Sun, Q.; Li, R.; Sham, T.-K.; Cui, X.; Sun, X. On Rechargeability and Reaction Kinetics of Sodium Air Batteries. *Energy Environ. Sci.* **2014**, *7*, 3747−3757.

DOI: 10.1021/acs.jpclett.5b00814
J. Phys. Chem. Lett. 2015, 6, 2027−2031